Atmos. Chem. Phys., 17, 7067–7081, 2017
https://doi.org/10.5194/acp-17-7067-2017

Atmospheric Chemistry and Physics
Open Access
EGU

Assimilation of satellite NO_2 observations at high spatial resolution using OSSEs

Xueling Liu[1], Arthur P. Mizzi[2], Jeffrey L. Anderson[3], Inez Y. Fung[1], and Ronald C. Cohen[1,4]

[1]Department of Earth and Planetary Science, University of California at Berkeley, Berkeley, CA, USA
[2]Atmospheric Chemistry Observations and Modeling Laboratory, National Center for Atmospheric Research, Boulder, CO, USA
[3]Institute for Mathematics Applied to Geosciences, National Center for Atmospheric Research, Boulder, CO, USA
[4]Department of Chemistry, University of California at Berkeley, Berkeley, CA, USA

Correspondence to: Ronald C. Cohen (rccohen@berkeley.edu)

Received: 26 August 2016 – Discussion started: 5 September 2016
Revised: 10 April 2017 – Accepted: 29 April 2017 – Published: 15 June 2017

Abstract. Observations of trace gases from space-based instruments offer the opportunity to constrain chemical and weather forecast and reanalysis models using the tools of data assimilation. In this study, observing system simulation experiments (OSSEs) are performed to investigate the potential of high space- and time-resolution column measurements as constraints on urban NO_x emissions. The regional chemistry–meteorology assimilation system where meteorology and chemical variables are simultaneously assimilated is comprised of a chemical transport model, WRF-Chem, the Data Assimilation Research Testbed, and a geostationary observation simulator. We design OSSEs to investigate the sensitivity of emission inversions to the accuracy and uncertainty of the wind analyses and the emission updating scheme. We describe the overall model framework and some initial experiments that point out the first steps toward an optimal configuration for improving our understanding of NO_x emissions by combining space-based measurements and data assimilation. Among the findings we describe is the dependence of errors in the estimated NO_x emissions on the wind forecast errors, showing that wind vectors with a RMSE below 1 m s^{-1} allow inference of NO_x emissions with a RMSE of less than 30 mol/(km^2 × h) at the 3 km scale of the model we use. We demonstrate that our inference of emissions is more accurate when we simultaneously update both NO_x emissions and NO_x concentrations instead of solely updating emissions. Furthermore, based on our analyses, we recommend carrying out meteorology assimilations to stabilize NO_2 transport from the initial wind errors before starting the emission assimilation. We show that wind uncertainties (calculated as a spread around a mean wind) are not important for estimating NO_x emissions when the wind uncertainties are reduced below 1.5 m s^{-1}. Finally, we present results assessing the role of separate vs. simultaneous chemical and meteorological assimilation in a model framework without covariance between the meteorology and chemistry.

1 Introduction

Weather and climate act in concert with emissions to establish the concentrations of chemicals and aerosols in the boundary layer. To understand the factors that affect public health and the productivity of agriculture and animal husbandry, we require accurate models of both emissions and the boundary layer meteorology to define the surface layer concentrations that determine the exposure of humans, animals, and plants to chemicals and aerosol. There remain substantial uncertainties in even the best models of emissions and even more so in the best models of boundary layer dynamics (for example, Hu et al., 2010). Current uncertainties in the surface NO_2 emission inventories in the US are thought to be of the order of 50 % (Krotkov et al., 2016; Travis et al., 2016). Comparable uncertainties affect estimates of the planetary boundary layer (PBL) height and mixing rates that redistribute emissions from the surface (Kretschmer et al., 2012, 2014; Lauvaux and Davis, 2014).

Over the last decade, there has been increased use of data assimilation techniques to constrain model forecasts and reanalyses of atmospheric constituents (e.g., Arellano Jr. et al., 2007; Edwards et al., 2009; Claeyman et al., 2011; Lahoz et al., 2012; Pagowski and Grell, 2012; Bowman, 2013; Gaubert et al., 2014; Hache et al., 2014; Saide et al., 2014; Zoogman et al., 2014; Barré et al., 2015; Bousserez et al., 2016; Mizzi et al., 2016). Assimilation of chemicals can be extended to optimize model inputs such as emissions, thereby providing insight into how to improve the processes that govern the model performance (e.g., Elbern et al., 2007; Barbu et al., 2009; Chatterjee et al., 2012; Miyazaki et al., 2012b; Koohkan et al., 2013; Yumimoto, 2013; Cui et al., 2015; Guerrette and Henze, 2015; Turner et al., 2015).

To date most efforts to incorporate satellite remote sensing in data assimilation have focused on long-lived chemicals such as CO, CH_4, or CO_2 and regional- and continental-scale aspects of emissions. Processes that govern variability in emissions within an urban center require new approaches that use models and observations with high spatial and temporal resolution. NO_2 has a lifetime of only a few hours and thus exhibits concentration changes that are substantial on spatial scales of 50–75 km. Observations of variations in NO_2 are thus uniquely suited to studying emissions and meteorology on city scales. Averaged measurements of NO_2 have been shown to be promising for evaluation of absolute emissions and trends (Russell et al., 2012; Miyazaki et al., 2016) as well as providing information on the coupling of boundary layer winds to chemical lifetime (Beirle et al., 2011; Valin et al., 2013). Current space-based instruments have resolution that is too low to provide direct information on lifetimes and emissions from a single overpass. Instead, analyses have focused on data averages, which wash out some of the key details about emission location and chemical lifetime.

New instruments with spatial resolution of a few kilometers will soon change that situation. The TROPOspheric Monitoring Instrument (TROPOMI, launch date in mid-2017) will be the first to provide spatial resolution sufficient to observe these NO_2 changes in a single overpass. TROPOMI will view the atmosphere from low Earth orbit and provide one image per day. We also anticipate the launch of three geostationary satellites, the Geostationary Environmental Monitoring Spectrometer (GEMS), the Tropospheric Emissions: Monitoring of Pollution (TEMPO), and Sentinel-4, which will provide observations at higher temporal resolution with hourly repeats at locations in Asia, North America, and Europe, respectively (Zoogman et al., 2017). The spatial resolution of these new low Earth orbit (LEO) and geostationary (GEO) instruments will be sufficient to provide ~ 10 samples within the advection distance that is determined by the chemical lifetime of NO_2. This dense sampling will permit characterization of multi-exponential or non-exponential behavior where current analyses are typically forced to assume single-exponential decay. To take full advantage of these measurements within a data assimilation system, we will need to model the NO_2 column at similar spatial resolution. This is both because the spatial scales of important variation in atmospheric plumes are of the order of 4 km and because of the steep nonlinearity in the lifetime of NO_2 as a function of the NO_2 concentration. For example, biases of 34 % (3.3 to 5.0×10^{15} molecules cm^{-2}) are found in the modeled averaged NO_2 column over Los Angeles at resolutions of 96 km compared to 12 km. For a point source, such as a power plant, model convergence is observed only at a grid resolution of 4 km or smaller (Valin et al., 2011).

In this study, we describe a chemical transport ensemble data assimilation system with high spatial and temporal resolution and simultaneous assimilation of meteorology and chemistry to adjust NO_x emissions on scales consistent with the temporal scale of NO_x evolution. We use this forecast–assimilation system to investigate the factors that influence the capability of TEMPO NO_2 observations to accurately constrain NO_x emissions. Our long-term goal is to estimate hour-to-hour variations in NO_x emissions on the scale of model grid point resolution (3 km) and to use these variations to understand the processes controlling the emissions. The remainder of this paper is organized as follows: in Sect. 2, we describe the forecast and data assimilation system, the system setup, observations, and the TEMPO NO_2 simulator – the simulation of column NO_2 that would be observed by TEMPO. In Sect. 3, we describe the experimental design, including a series of assimilation experiments that guide optimization of the emission estimation performance. In Sect. 4, we assess the performance of meteorology and chemistry assimilation. We then discuss the results and provide insight into the potential accuracy of NO_2 emission fields derived from geostationary NO_2 observations. We present our conclusions in Sect. 5.

2 The data assimilation system

The forecast–data assimilation system used here is WRF-Chem/DART (Data Assimilation Research Testbed) as described by Mizzi et al. (2016). It consists of the following elements: the forecast model, the assimilation engine, and observations of meteorological and chemical states to be assimilated.

2.1 WRF-Chem model description

The core meteorological and chemical forecast model is the regional online chemical transport model (CTM) WRF-Chem v3.4.1 (www2.acd.ucar.edu/wrf-chem). The model domain is a one-way nest with an outer domain of 12 km resolution covering western North America and an inner domain of 3 km resolution focused on the city of Denver, CO (Fig. 1). The 3 km resolution domain is 660 km by 840 km. The model has 30 vertical levels between the surface and an upper boundary of 100 mb and 10 levels within the bound-

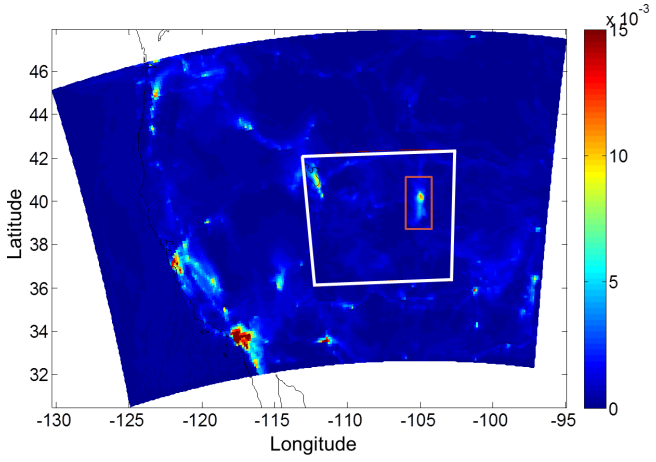

Figure 1. Model domain setup with 12 km outer domain and 3 km inner domain (white square). Data assimilation is performed for the inner domain. Meteorological observations in the inner domain are assimilated. TEMPO NO_2 observations inside the red rectangle are assimilated.

ary layer ($\sim$ 1.5 km). Simulations of meteorology in the outer domain are initialized and constrained at the lateral boundary by North American Regional Reanalysis (NARR) data from National Centers for Environmental Prediction (NCEP). The NARR data have a native horizontal resolution of 32 km with 45 pressure levels and 3 h temporal resolution. We use the global chemical model output from MOZART to initialize the chemical simulation in the outer domain and to provide the chemical boundary condition. After a spin-up time of 4 days for the outer domain, the inner domain simulation is initialized and constrained through one-way nesting in both meteorology and chemistry.

Anthropogenic emissions for WRF-Chem are from the National Emissions Inventory (NEI) 2011 version 1 at native $4 \times 4\,km^2$ resolution. The NEI 2011 provides hourly-varying emissions for a typical weekday in summertime. The emissions do not vary from day to day. Biogenic emissions are calculated online with the simulation results by the Model of Emissions of Gases and Aerosols from Nature (MEGAN). Fire emissions are not included. We use the widely used regional acid deposition model version 2 (RADM2) as the gas-phase chemical mechanism (Stockwell et al., 1990). There are 59 species and 157 reactions to represent both inorganic and organic chemical reactions under tropospheric conditions. It includes the chemical losses of NO_x through reaction with OH radical to form nitric acid, and other NO_x sinks such as peroxyacyl nitrates and alkyl nitrate.

2.2 DART ensemble assimilation system

WRF-Chem/DART is a regional multivariate data assimilation system developed by the National Center for Atmospheric Research (NCAR) to analyze meteorological

Table 1. The experimental setup of each assimilation run. The three ensemble runs assimilate NO_2 observations every hour and differ in treatment of meteorology forecast.

Experiment	Met assim	Chem assim	Note
REF	No	Yes	True meteorology
ENS.1	Yes	Yes	Ensemble of meteorology and chemistry
ENS.2	Yes	Yes	Only update emissions
ENS.3	Yes	Yes	Initial meteorology ensemble is from the next day
REA	No	Yes	Using ensemble mean from ENS.1

Table 2. DART configurations.

Parameter	Value
Filter type	EAKF
Adaptive inflation	1.0, 0.6 (initial mean, spread)
Inflation damping	0.9
Adaptive localization threshold	2000
Localization type	Gaspari–Cohn
Horizontal localization half-width for meteorology (chemical) observation	50 km (10 km)
Outlier threshold	3.0
Ensemble members	30

variables and chemical variables simultaneously (Mizzi et al., 2016). We use the ensemble adjustment Kalman filter (EAKF) in DART to analyze the states with an ensemble size of 30. Details of the EAKF algorithm and its implementation in DART are documented in Anderson, 2001; Anderson and Collins, 2007; and Anderson et al., 2009. In this study the system is extended to assimilate synthetic TEMPO NO_2 column observations. As emissions are not prognostic variables of the forecast model, we implement a state augmentation approach to include emissions in the state variables (Aksoy et al., 2006). The chemical state variables include the NO_2 concentration and NO_x emissions. Based on the settings used in meteorology data assimilation, the meteorological state variables are U, V, W, T, QVAPOR, QCLOUD, QRAIN, QICE, and QSNOW. MU and PH are used in vertical coordinate transforms. $T2$, $Q2$, $U10$, $V10$, and PSFC are used for surface data assimilation forward operators. Definitions of these variables are taken from Romine et al. (2013) and are given in the Appendix. Adaptive spatially and temporally varying inflation is applied to the prior state to assist in maintaining the ensemble spread. We summarize the DART configuration details in Table 2.

2.2.1 Spatial localization

In ensemble methods the correlations among spatially remote variables in the prior ensemble are regarded as spurious correlations due to the small ensemble size (30). To compensate for this under-sampling issue, spatial localization is introduced to reduce the prior correlations based on the distance between the observed and modeled state variables (Houtekamer and Mitchell, 2001). In this study, we apply the fifth-order distance-dependent Gaspari and Cohn (GC) function (Gaspari et al., 1999) to reduce the spurious impact of observations on spatially remote state variables. The scaling distance in the GC function is defined by a half-width parameter, 2 times of which is the distance where the GC function reaches zero. With a data assimilation window of 1 h and a maximum wind speed of 3–5 m s^{-1}, an observation of column NO_2 primarily reflects information about emissions that occurred during the last hour and within 10 km. We use the half-width distance in spatial localization as 10 km and demonstrate this as the optimal value based on sensitivity experiments with localization distances of 5, 10, 20, and 50 km. Because of the high density of TEMPO NO_2 observations ($2 \times 4.5\,km^2$), the update of chemical state variables is mostly determined by the local observations.

2.2.2 Variable localization

Similar to the concept of spatial localization, variable localization techniques have been introduced (Arellano Jr. et al., 2007) to reduce spurious correlations among observations and different types of state variables. For example, for CO_2 flux estimation, Kang et al. (2011) showed that the performance of data assimilation using a variable localization that zeroes out the prior error covariance between meteorological variables and CO_2 flux is better than using a standard full covariance approach. Here we isolate the influence of meteorological observations on chemical variables and vice versa.

2.3 Initial and boundary condition ensemble

We generate the initial chemical ensemble by adding the perturbations to the mean state of the fine domain forecast. In the ensemble method the generated ensemble should represent the error statistics of the initial guess of the model state (Evensen, 2003). The correlation between perturbations of chemical state variables is modeled by a simple isotropic exponential decay function with a characteristic correlation length of 50 km. For the meteorology ensemble, random perturbations were added to each member by sampling the NCEP background error covariance using the WRF Data Assimilation System (WRFDA; http://www2.mmm.ucar.edu/wrf/users/wrfda) (Barker et al., 2012). The options used for the WRFDA settings are summarized in Table 3. The parameter cv_option indicates the background error options in WRFDA. With a cv_option = 3, we use the NCEP background error covariance, which is estimated in grid space by what has become known as the National Meteorological Center (NMC) method. The statistics are estimated with the differences of 24 and 48 h global forecast system (GFS) forecasts with T170 resolution, valid at the same time for 357 cases, distributed over a period of 1 year. The parameter je_factor is the ensemble covariance weighting factor. This factor controls the weighting component of ensemble and static covariances. The ensemble member lateral boundary condition perturbations are generated in a similar manner to the initial ensemble using the fixed-covariance perturbation technique. The boundary condition for the analysis time is adjusted to match the analysis from DART. The tendencies for the later times in the forecast are adjusted to match the change in the boundary condition for the analysis time.

Table 3. WRFDA configurations.

Parameter	Value
cv_options	3 (NCEP background error model)
je_factor (ensemble covariance weighting factor)	1.0

2.4 Emission update scheme

By including emissions in the ensemble state vector, emissions are estimated as hourly evolving parameters. Estimation of time-evolving emissions using data assimilation was first presented for carbon flux estimation (Kang et al., 2011, 2012). Such an approach provides emission information beyond an average for a specific time period. NO_x emissions within cities show significant variation within the urban core and between the urban core and the surrounding suburbs. The observed columns show strong spatial variation dominated by an emission hotspot that results from the combination of spatial patterns in emissions and the short chemical lifetime. The goal of this work is to constrain hourly evolving emissions at the native model resolution. Here we start with a simple case in which the emission error is a constant fraction at all times of the day with the prior emissions set as 70 % of the true emissions and we investigate the ability of assimilation to recover the original emissions.

A challenge for updating the emissions in the augmented state vector is the absence of an emission forecast model to evolve the emission variables forward in time. The bottom-up inventory to be optimized provides hourly-resolved emissions for each model grid point. Instead of treating the emission variables of each hour at a specific location as independent parameters, we update the emission scaling factors at each assimilation cycle. In our emission update scheme, the TEMPO NO_2 observations at time i are assimilated to generate a scaling factor for emissions at time $i-1$. In this way,

the model–observation difference in the NO_2 column will correct the emission of an hour ago instead of the current emission. This approach is reasonable because errors in NO_2 concentration result from errors in previous emissions. Considering the short NO_2 lifetime of 3 h in summer daytime, emissions from the previous hour have a large contribution to the NO_2 total mass at the current time. For a given model grid point, we define the true (e^{t}_{i-1}), prior (e^{prior}_{i-1}), and posterior (e^{post}_{i-1}) emissions at time $i-1$. Since we start the assimilation with 70 % of the true emissions, we have $e^{prior}_{m} = 0.7e^{t}_{m}$ for any time m. After assimilating observations at time i, we compute the scaling factor (S_{i-1}) for emissions at time $i-1$ as follows: $S_{i-1} = e^{post}_{i-1}/e^{prior}_{i-1}$. Then we update the prior emissions at time i as $e^{prior}_{i} = S_{i-1} \times e^{prior}_{i}$. This prescription enables us to derive spatial 2-D emission scaling factors, which play the role of emission forecast models.

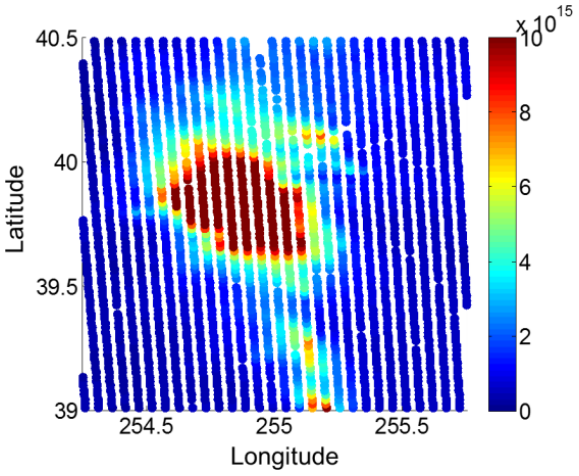

Figure 2. Example of synthetic TEMPO NO_2 column observations over Denver, CO, at 17:00 MST on 2 July 2014.

2.5 Synthetic meteorological and chemical observations

Assimilated observations include meteorological observations and NO_2 column retrievals from the TEMPO observing system simulation experiments (OSSE). For meteorological observations, we assimilated synthetic observations of temperature, wind, and humidity from the NCEP Meteorological Assimilation Data Ingest System (MADIS) (https://madis.noaa.gov/). MADIS is a meteorological observational database and data delivery system that provides observations that cover the globe. MADIS ingests data from NOAA data sources and non-NOAA providers, decodes the data, and then encodes all of the observational data into a common format with uniform observational units and time stamps. For wind observations, the assimilated observation types include standard aviation routine weather reports (METAR), wind profilers, aircraft-based observations (ACARS), national mesonet data, and satellite data. Among these, the mesonet wind data are the most abundant, with ~ 1000 observations located in the mapping domain in Fig. 2. The observation errors are the default values from the DART facility that are defined based on NCEP statistics (Romine et al., 2013).

The Geostationary Coastal and Air Pollution Events (GEO-CAPE) mission (Fishman et al., 2012) aims at improving our understanding of both coastal ecosystems and air quality from regional to continental scales. As the first phase of the GEO-CAPE implementation, TEMPO (Zoogman et al., 2017), launch date circa 2019, will provide hourly measurements of NO_2, HCHO, tropospheric ozone, aerosols, and cloud parameters during the daytime. TEMPO will measure solar backscattered light in the UV–visual spectral range. Implemented on a geostationary platform, TEMPO retrievals will achieve hourly observations of NO_2 vertical column density (VCD) at a native spatial resolution of 2×4.5 km during the daylight period. TEMPO's high spatiotemporal resolution will allow a more detailed assessment of emission inventories, e.g., urban-scale and large power plant NO_2 emissions and mobile emissions that show significant spatial and temporal variations due to urban transit patterns, than is possible with existing LEO observations.

As TEMPO has not been launched yet, we generate synthetic TEMPO NO_2 observations by simulating the instrument's observing characteristics. We carried out a model run, i.e., a forward integration of WRF-Chem for the period from 2 July to 7 July 2014 with NO_2 emissions specified by NEI 2011 (true). In the NO_2 retrieval algorithm, a layer-dependent box-air-mass factor (BAMF) represents the sensitivity of the retrieved NO_2 in a specific layer to the true value in the atmosphere. The BAMF of NO_2, as an optically thin absorber, is a vector and determines the measurement sensitivity to NO_2 molecules at 35 pressure levels. In the calculation of BAMFs, we follow the latest version of the NASA standard product retrieval (level 2, version 2.1, collection 3) algorithm (Bucsela et al., 2013) assuming the TEMPO measurement has similar characteristics to the Ozone Monitoring Instrument (OMI). We assume clear-sky conditions for all observing scenes. Cloudy-sky scenes affect only the number of observations available as the cloudy scenes are usually discarded in the data filtering process. Without running a radiative transfer code, the elements of the BAMF vector are computed as a function of solar zenith angle (SZA), viewing zenith angle (VZA), relative azimuth angle (RAA), terrain reflectivity (Rt), terrain pressure (Pt), atmospheric pressure level (p), and the NO_2 profile (Bucsela et al., 2013). The viewing parameters are computed by simulating the viewing geometry based on the location of ground pixels in relation to the observing instrument. The geometry-related parameters (SZA, VZA, and RAA) are computed hourly for each TEMPO observation using Matlab functions sun_position.m and geodetic2aer.m with inputs of the location and time of each TEMPO observation, and

Table 4. Relative observation uncertainty σ_{rel} in synthetic TEMPO NO_2 column for each scenario.

Type	NO_2 column	Gaussian distribution
Clean	$< 0.3 \times 10^{15}$ molec. com^{-2}	N (200 %, 100 %)
Polluted	$\geq 0.3 \times 10^{15}$ molec. com^{-2}	N (7.5 %, 2.5 %)

the location (36.5° N, 100° W) and altitude (35 786 km) of the TEMPO sensor. The terrain reflectivity and terrain pressure are sampled from the WRF-Chem nature run (NR; see Sect. 3) for each TEMPO pixel. All the parameters have an hourly frequency consistent with the TEMPO temporal observation pattern. Consequently, the NO_2 profile with high spatiotemporal resolution captures the diurnal variation in NO_2 and its urban–rural contrast. This contrast is essential to accurate interpretation of the measured spectrum (Russell et al., 2011; Laughner et al., 2016).

To generate synthetic TEMPO data, the modeled 3-D concentration fields from the NR are sampled in as similar a manner to the planned TEMPO measurements as the transport model permits: using the computed BAMF vertically, hourly frequency, 2×4.5 km nadir resolution and variations following the Earth's curvature horizontally. Figure 2 shows an example of the spatial distribution of TEMPO data over Denver, CO.

We describe the observation error as a relative value (σ_{rel}) and a random draw from a Gaussian distribution to avoid using a fixed value. The magnitude of the relative mean uncertainty of the NO_2 column is different between clean and polluted areas (Boersma et al., 2004). We follow their categorization of clean versus polluted regions and summarize the mean and standard deviation of a Gaussian distribution for each scenario in Table 4. For polluted regions, we give a mean uncertainty of 7.5 %, which is lower than the 35 % minimum in the OMI NO_2 retrievals. First, most of these errors are systematic, affecting comparison of different cities, but have smaller variation across a single, small-area scene of observations. Second, a relatively lower observation error improves the efficiency of data assimilation and helps to examine the sensitivity to other parameters. Finally, as TEMPO is expected to be operational no sooner than 2018, it is reasonable to expect that the retrieval error that is dominated by the air mass factor (AMF) in regions with large columns will be reduced as a result of future improvements in AMF simulation (Laughner et al., 2016). The synthetic observations assimilated are obtained by sampling the NR using the TEMPO observation simulator and adding observation error as $y^{obs} = N(y^{tr}\sigma^2)$, where y^{tr} are the TEMPO NO_2 observations sampled from the true emissions, and σ is the observation error standard deviation computed as $\sigma = y^{tr} \times \sigma_{rel}$.

3 Assimilation experiments

We begin by performing OSSEs in the context of a perfect model. The original NEI 2011 is used as the emission input for the NR without any emission perturbation. We consider the NR as the true atmosphere and sample meteorological and NO_2 observations from the NR. The control run (CR) is a parallel model calculation to the NR and suffers from imperfect model input and parametrization. The differences between the NR and the CR in this study are the emission inputs and the initial conditions for the meteorology. We begin by creating a NR and a CR simulation in the outer domain of 12 km resolution (d01) without assimilating observations using a simulation setup as described above in Sect. 2.1. We impose a difference to the CR by using emissions in the CR that are scaled to be 70 % of the NR emissions. We apply the identical forecast model (WRF-Chem) for both the NR and the CR to isolate the behavior of the ensemble filter algorithm from the influence of the model errors. Then the NR and the CR in the inner domain of 3 km (d02) are initialized from the corresponding d01 simulations at 06:00 MST on 2 July 2014. At the time of initialization, the NR and CR on d02 share the same meteorological fields and differ in NO_x concentrations due to different emission inputs. Our next step is to generate a 30-member ensemble from the CR. We use WRFDA to generate an ensemble in meteorological variables (Barker et al., 2012). For chemical states, we give an ensemble in NO_x emissions and concentrations using the method described above in Sect. 2.3. The forecast of the CR ensemble is the prior estimate of the states and will be combined with the observations in the assimilation cycle to yield the posterior states. By comparing the posterior emissions with the true emission, we evaluate the data assimilation performance. We run assimilation experiments from 10:00 MST 2 July 2014 to 18:00 MST 5 July 2014 with an assimilation window of 1 h. We assimilate $\sim 20\,000$ weather observations in each assimilation window and ~ 9000 TEMPO NO_2 column observations in each daytime assimilation window.

We design a series of experiments to explore the optimal approach to estimating NO_x emissions as shown in Table 1. In all experimental runs, we bias the CR initial emissions to be 30 % below the reference emissions and examine the ability of the assimilation to recover the reference emissions. First, a reference assimilation run (REF) is conducted without including the meteorological ensemble so that the NR and CR ensembles have identical meteorological simulations. This shows the best-case scenario to constrain emissions, assuming no errors associated with meteorology. In practice, the modeled meteorology is different from the true atmosphere due to errors in the model initial conditions, parameterizations, and resolutions. In a more realistic simulation case labeled as ENS, we initialize both the meteorology and the NO_x emissions using an ensemble in which both weather observations and TEMPO NO_2 columns are assimilated. In ENS.1 the CR ensemble is generated by adding per-

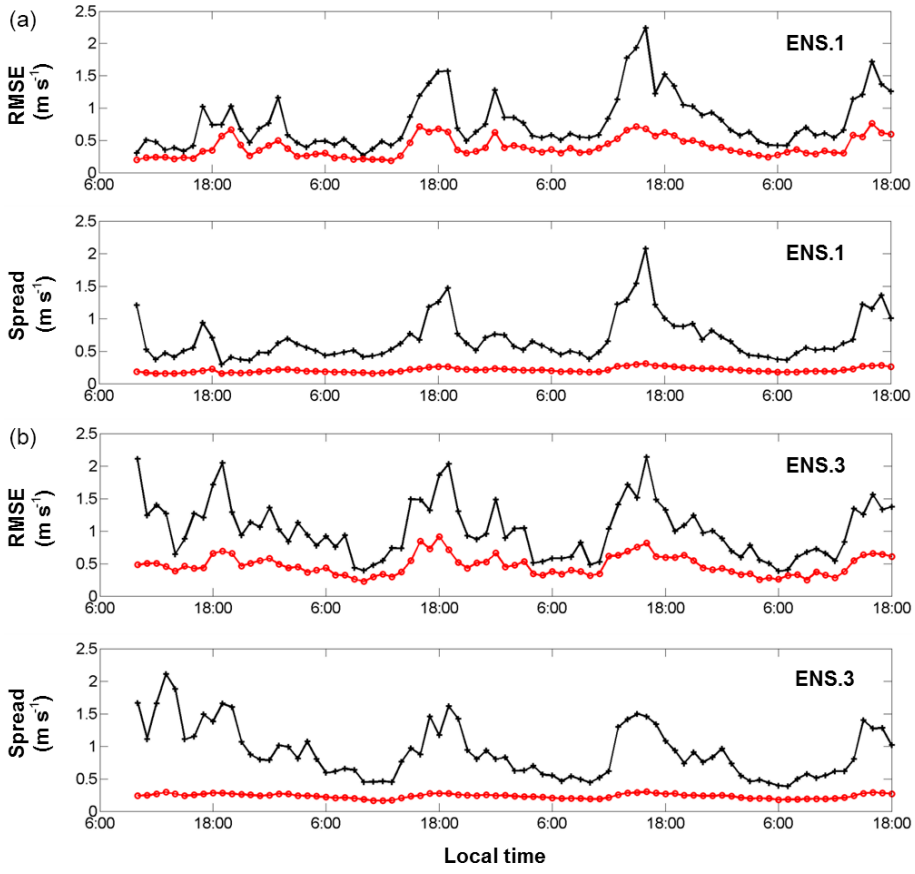

Figure 3. Time evolution of prior (black) and posterior (red) RMSEs and spreads of surface mesonet zonal wind observation in Denver from 2 July 10:00 to 5 July 18:00 for ENS.1 **(a)** and ENS.3 **(b)**.

turbations to the CR mean state. In this example, the CR ensemble mean meteorology is very close to the NR because CR and NR differ in NO_x emissions only. For the chemistry, the assimilated TEMPO NO_2 observations are allowed to update both the NO_2 concentration and the NO_x emissions every hour. In ENS.2 we allow NO_2 observations to update NO_x emissions but not the NO_x concentrations and keep the meteorology assimilation the same as ENS.1. By comparing ENS.1 and ENS.2 we evaluate the additional benefits of updating concentrations when observations are assimilated to constrain emissions. In ENS.3, we use the meteorology of the next day to initialize the CR ensemble so that there is some difference between the CR ensemble mean and the NR in the meteorology. To be specific, the CR meteorology ensemble on 3 July 2014 09:00 MST is used as the CR ensemble on 2 July 2014 09:00 MST. This is to mimic our imperfect knowledge of the atmospheric state and its uncertainty. ENS.1 and ENS.3 differ only in the meteorology of the initial ensemble. By comparing these two runs, we evaluate the sensitivity of the NO_2 assimilation to the initialization of the meteorology. Our final experiment, REA, mimics a general approach to a chemistry-only data assimilation where the meteorology is extracted from an existing reanalysis. REA reinitializes the meteorological state every hour with the best estimate of meteorological states generated by ENS.1. By design, REA has a single run of meteorology but uses an ensemble of NO_2 emissions and concentrations that are affected by assimilation of TEMPO NO_2 observations. As in ENS.1, REA includes simultaneous updates to emissions and concentrations.

4 Results

We evaluate the assimilation result by comparing with the NR states. We calculate the RMSE of observed quantities by $\sqrt{\sum_i^n (y_i^{\mathrm{m}} - y_i^{\mathrm{t}})^2/n}$, where y_i^{m} and y_i^{t} are the model and true values for the ith observation, respectively, and n is the total number of observations of interest. We also calculate the RMSE of model states by $\sqrt{\sum_i^n (x_i^{\mathrm{m}} - x_i^{\mathrm{t}})^2/n}$, where x_i^{m} and x_i^{t} are the model and true states at the ith model grid point, respectively, and n is the total number of grid points of interest. For the wind variable, the grid points of interest are all the points located within a sub-model space as shown in

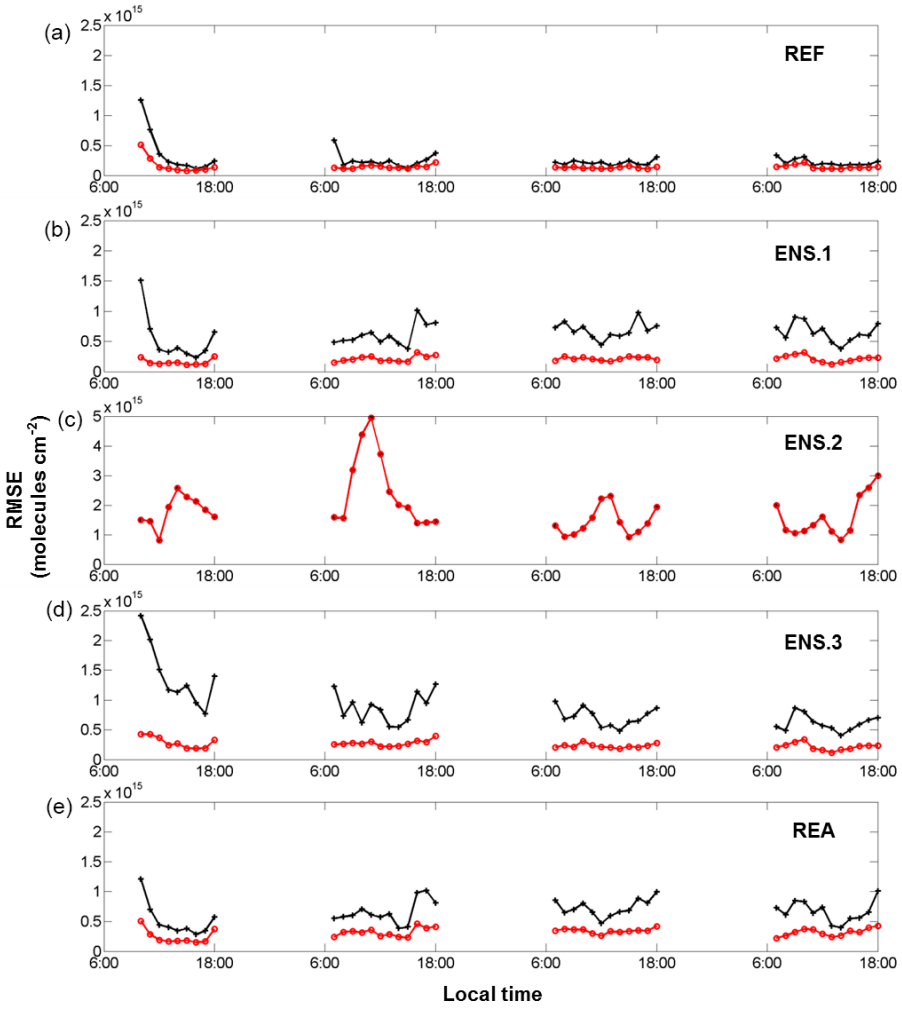

Figure 4. Time evolution of prior (black) and posterior (red) RMSEs of Denver TEMPO NO_2 column observation from 2 July 10:00 to 5 July 18:00 for REF, ENS.1, ENS.2, ENS.3, and REA (from **a** to **e**).

Fig. 2, containing the lowest 10 model levels vertically. Because NO_x is located mostly in the boundary layer, the NO_2 transport error is determined by the meteorological errors in the lowest 10 model levels. For NO_x emission variables, the grid points of interest are categorized as emission points with emissions greater than 50 mol/(km^2 × h). Our analysis does not include emissions below 50 mol/(km^2 × h) because the observations over such low-emission regions have large uncertainty and are not constrained. We also analyze the uncertainty of the prior and posterior estimates. The uncertainty is expressed by the 1-σ standard deviation of the ensemble.

4.1 Wind assimilation

The success of ensemble-based assimilation relies on how well the ensemble system represents the uncertainty. One way to test the success of an OSSE is to compare the RMSE computed with respect to the true observations with the ensemble spread directly. Figure 3 shows the evolution of the RMSE and spread for mesonet observations of zonal wind for ENS.1 and ENS.3. Overall, for each experiment the variation and magnitude of prior ensemble spread are similar to those of the prior RMSE, indicating that the ensemble develops a good amount of spread for the success of OSSE.

We find that the errors in the observation space of mesonet winds are reduced by 50 % on average from the prior to the posterior estimates. The prior wind RMSE exhibits the peaks in the afternoon and this results in the largest error reduction. The posterior wind RMSE shows a temporal average of 0.39 and 0.47 m s^{-1} in ENS.1 and ENS.3, respectively. Because ENS.1 is initialized with a meteorology ensemble with its mean close to the true ensemble, the wind RMSE on the first day is low and gradually grows to about 1 m s^{-1}. In contrast, the prior wind RMSE in ENS.3 is as high as 2 m s^{-1} on the first day as a result of using an initial meteorology ensemble that is very different from the true ensemble. The wind RMSE evolution in the two experiments becomes very similar after the afternoon of the third day of assimilation,

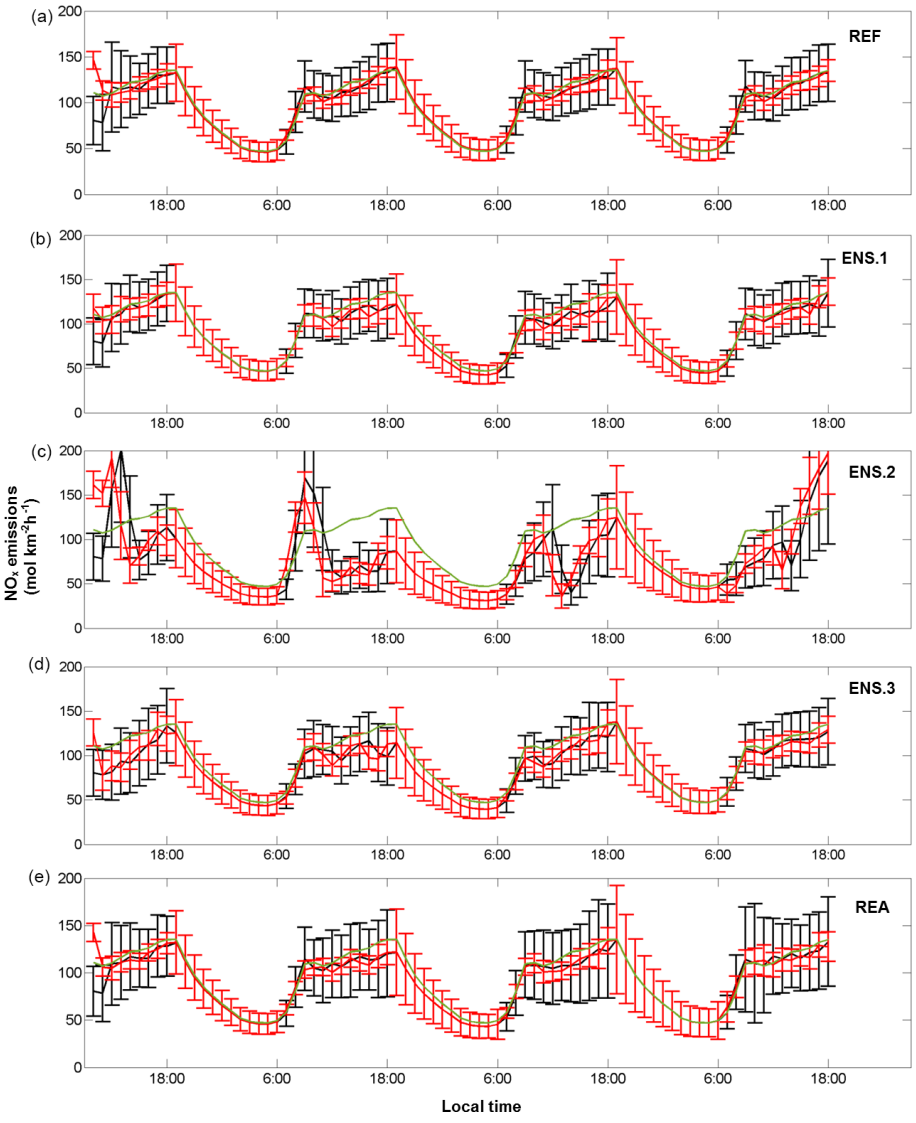

Figure 5. Time evolution of averaged Denver prior (black), posterior (red), and true (green) emissions for REF, ENS.1, ENS.2, ENS.3, and REA (from **a** to **e**).The error bar is defined by the ensemble spread and represents the uncertainty of the prior and posterior estimates.

4 July 2014. We conclude that the ensemble wind assimilation system performance is independent of the initialization approach after the first day.

4.2 TEMPO NO_2 assimilation

We assimilate hourly TEMPO NO_2 column observations and take their difference with the modeled column to correct the predicted NO_2. Figure 4 shows the TEMPO NO_2 column RMSE evolution for all experiments. With perfect knowledge of meteorology, REF shows significant reduction in TEMPO NO_2 RMSE in the first three update cycles and succeeds in recovering the true emissions (Fig. 5). The prior TEMPO NO_2 RMSE in the last 3 days varies below 3×10^{14} molecules cm^{-2} as a result of perfect NO_2 transport and improved emissions. This ideal case with the assumption of perfect meteorology sets the upper limit of error reduction in NO_2 concentrations by assimilating the TEMPO NO_2 observations. Compared with REF, ENS.1 shows a prior TEMPO NO_2 RMSE of 5–10×10^{14} molecules cm^{-2} due to the errors in NO_2 transport and emissions. By assimilating NO_2 observations, the TEMPO NO_2 RMSE is reduced by more than 50 % from the prior to the posterior emissions, indicating the potential of TEMPO NO_2 observations to improve the modeled atmospheric NO_2 composition for the chemical reanalysis product. Without updating the NO_2 concentrations in ENS.2, there is no reduction in the TEMPO NO_2 RMSE as expected. We find that the TEMPO NO_2 RMSE varies above 1×10^{15} molecules cm^{-2}, being the largest among all experiments because the emission estimations show very poor re-

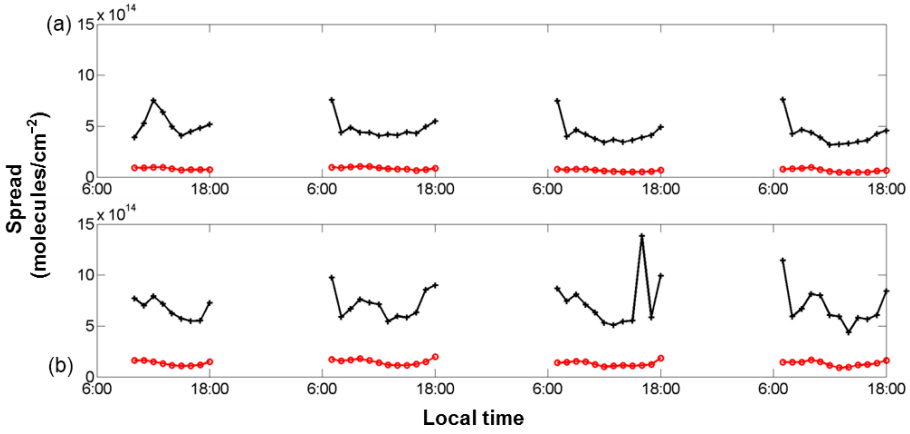

Figure 6. Time evolution of prior (black) and posterior (red) spreads of Denver TEMPO NO_2 column observation from 2 July 10:00 to 5 July 18:00 for REF **(a)** and ENS.1 **(b)**.

sults (shown in Sect. 4.3). The TEMPO NO_2 RMSE development in ENS.3 is very similar to ENS.1 except for the first day when ENS.3 shows higher errors in the wind field, which contribute to the NO_2 transport errors. We find that the NO_2 forecast using a single meteorology field in REA is very similar to the ensemble NO_2 forecast in ENS.1. This is because there is very little difference between the 1 h meteorology forecast and the ensemble forecast. In addition, the emission estimation results are also very similar. This is different from the previous study on CO_2 forecasts, which showed that for a 6 h forecast, the CO_2 transport driven by a single meteorological field has weaker vertical mixing and a stronger CO_2 vertical gradient when compared to the mean of the ensemble CO_2 forecasts initialized by the ensemble meteorological field (Liu et al., 2011).

We compare the TEMPO NO_2 column spread in REF and ENS.1 in Fig. 6. For both experiments, the prior NO_2 column spread varies with a magnitude that is similar to the prior RMSE (Fig. 4), which is the range desired for the NO_2 ensemble spread. The NO_2 forecast uncertainty represented by the NO_2 ensemble spread results from the uncertainties in NO_2 transport and emissions since the uncertainties in chemical production and removal processes are not included in this study. The uncertainties in NO_2 transport are determined by the prior wind ensemble spread, which is widest in the afternoon and stays as low as $\sim 0.5\,\mathrm{m\,s^{-1}}$ at other times for zonal wind (Fig. 3). The prior NO_x emission uncertainties are 60 % after inflation (Fig. 5). Under these circumstances, the mean prior TEMPO NO_2 column spread is 4.55×10^{14} molecules $\mathrm{cm^{-2}}$ in REF, which does not include NO_2 transport uncertainties, and is 7.03×10^{14} molecules $\mathrm{cm^{-2}}$ in ENS.1, which takes uncertainties in transport and emissions into account. The difference indicates that NO_2 transport contributes to 35 % of the total NO_2 forecast uncertainties in our assimilation setup. The TEMPO NO_2 column spread in REF is very stable because it is determined by the constant emission spread of 60 %. ENS.1 shows fluctuations in the evolution of TEMPO NO_2 column spread, which corresponds to the wind spread variation, with increasing spread in the afternoon.

4.3 NO_x emission estimation

We show the time evolution of the averaged urban emissions for all experiments in Fig. 5. For all experiments, the posterior emission ensemble spread is reduced compared to the prior spread, suggesting the effectiveness of assimilated NO_2 columns in constraining the emission uncertainties. In making these comparisons, we ignore the emission correction of the first assimilation cycle since the first update produces a significant overcorrection to emissions because of the accumulated underestimation of the NO_2 concentrations. By neglecting the first update, the prior emission ensemble mean of the second cycle is still 70 % of the true emission ensemble mean. During the nighttime when TEMPO observations are not available, we calculate the ratio of the posterior to true ensemble mean in the last cycle of daytime and use this together with the true nighttime emissions to derive the ensemble mean for the nighttime emissions. The prior and posterior emission ensembles of each nighttime hour are the same.

Not surprisingly, under the condition of perfect knowledge in meteorological fields, assimilating TEMPO NO_2 observations successfully improves the emissions within the first few updates. The estimated emissions agree well with the true emissions throughout the assimilation period. This demonstrates the capability of a geostationary NO_2 column observation system to constrain city-scale emissions and the reliability of the ensemble-based assimilation method to project the observed information to emissions.

We find that the errors in estimated emissions correlate with the wind errors. In ENS.1, the posterior emission is corrected to the true emission at the second cycle and stays close to the true emission throughout the first day. The good performance on the first day benefits from an initial meteo-

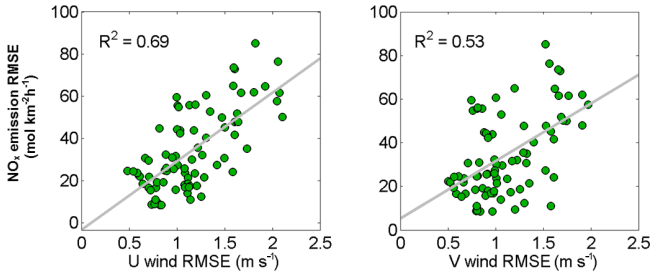

Figure 7. The scatter plot between the prior RMSE of boundary layer wind vectors and urban NO_x emission posterior RMSE over the 4-day daytime assimilation time period in ENS.1.

rology ensemble with its mean close to the true ensemble. For the following 3 days, the emission estimates succeed in recovering the true emissions during the morning and show deviations from the true emissions in the afternoon as a result of the increased error in boundary layer winds. Figure 7 shows the dependence of errors in the inverted emissions to the prior wind RMSE. The emission errors show high sensitivity to the wind errors, with a slope of the regression line of $32.5\,\mathrm{mol}\times\mathrm{km}^{-2}\mathrm{h}^{-1}\,/\,(\mathrm{m}\times\mathrm{s}^{-1})$. With a RMSE of model-predicted wind vectors of $1\,\mathrm{m\,s}^{-1}$, the errors in the estimated emissions are $30\,\mathrm{mol}\times\mathrm{km}^{-2}\,\mathrm{h}^{-1}$ on average. For the daytime cycles, the prior emission ensemble spread after inflation is approximately 60 % and is reduced by more than half after assimilation (Fig. 5). Even though the posterior ensemble mean does not match with the true ensemble mean in the afternoon, the true ensemble mean falls within the range of the posterior ensemble spread with a few exceptions.

We find that the simultaneous update of emission and concentration performs better than the emission-update-only scheme with an hourly assimilation window. ENS.2 is a parallel assimilation run with ENS.1 but updates emissions only. As shown in Fig. 5, the estimated emissions have very large differences from the true emissions and the posterior ensemble spread does not cover the true emissions. For example, at 10:00 MST on 3 July, the posterior ensemble mean (red) is very close to the true emissions. As a result of this, we have a very good prior ensemble estimate (black) at 11:00. However, the posterior emission at 11:00 is largely underestimated compared with the true emissions. This is because the posterior emissions from 07:00 to 09:00 are overestimated, which results in overestimated NO_2 concentrations at 10:00 and 11:00. As a result, even though the prior emissions from 10:00 to 11:00 are good, the model still overestimates NO_2 at 11:00 due to the NO_2 overestimation at 10:00. Without updating the concentrations, the observed differences in NO_2 columns are dominated by the NO_2 concentration errors of an hour ago and should not be attributed to the emissions.

We also find that the emission estimation should start after the meteorology assimilation becomes stable. As a comparison to ENS.1, ENS.3 is initialized with a meteorology ensemble that is very different from the true emissions. On the first day, the prior wind RMSE varies from 1 to $2\,\mathrm{m\,s}^{-1}$ (Fig. 3) and leads to enhanced NO_2 transport errors. As a result, the emission estimations are not successful for the first day. After the afternoon of the second day (3 July), the wind RMSE evolution is similar between ENS.1 and ENS.3 and as a result, the emission estimations perform in a similar way. We recommend allowing meteorology assimilations to stabilize from the initial transport errors before assimilating chemical observations to constrain the emissions.

With an hourly re-initialization of meteorology, the NO_2 transport error statistics are not important to emission estimation if the current practice of using a single meteorological field to transport NO_2 is adopted. The emission estimation performance in REA is very similar with that in ENS.1 (Fig. 5). This is because the difference in the 1 h NO_2 forecast driven by an ensemble meteorological field and a single ensemble mean field is very small. Though the wind uncertainties represented by the meteorological ensemble reach $1.5\,\mathrm{m\,s}^{-1}$ in the afternoon, our results show that the information of wind uncertainties is not important for estimating NO_x emissions.

Finally, we examine the emission estimation performance in ENS.1 at the scale of the model grid (3 km). As shown in Fig. 8, the true emission shows high spatial variation from the city center to the suburbs as well as distinct point emission sources. In the example of the emission estimate at 09:00, the posterior emission recovers the true emission very well with the posterior RMSE of $21.6\,\mathrm{mol/(km^2\times h)}$. In contrast, the emission estimate at 16:00 shows a RMSE of $46.5\,\mathrm{mol/(km^2\times h)}$ due to relatively high wind errors. The posterior emission underestimates the emissions significantly all over the city except for the regional overestimation in the east. The emission hot spot of $\sim 250\,\mathrm{mol/(km^2\times h)}$ in the city center is not fully represented in the posterior estimate. In conclusion, when wind errors are low, the difference between posterior emission and the true emission can be reduced to $\pm 25\,\mathrm{mol/(km^2\times h)}$ at most grid points. With high wind errors, this difference varies significantly from point to point and grows as large as $100\,\mathrm{mol/(km^2\times h)}$.

5 Summary and conclusions

In this study, we explore an approach to estimating NO_x emissions by assimilating column NO_2 and meteorological observations in a system comprised of the regional CTM, WRF-Chem, and the DART EAKF. This ensemble-based data assimilation system allows the flexibility to assimilate observations of meteorological and chemical variables on various scales of space and time. Our approach anticipates the future availability of long-term measurements, high spatial resolution, and frequent repeats of multiple species from satellites such as TEMPO.

Previous work has shown that NO_x concentrations and columns vary at fine scales, necessitating high spatiotem-

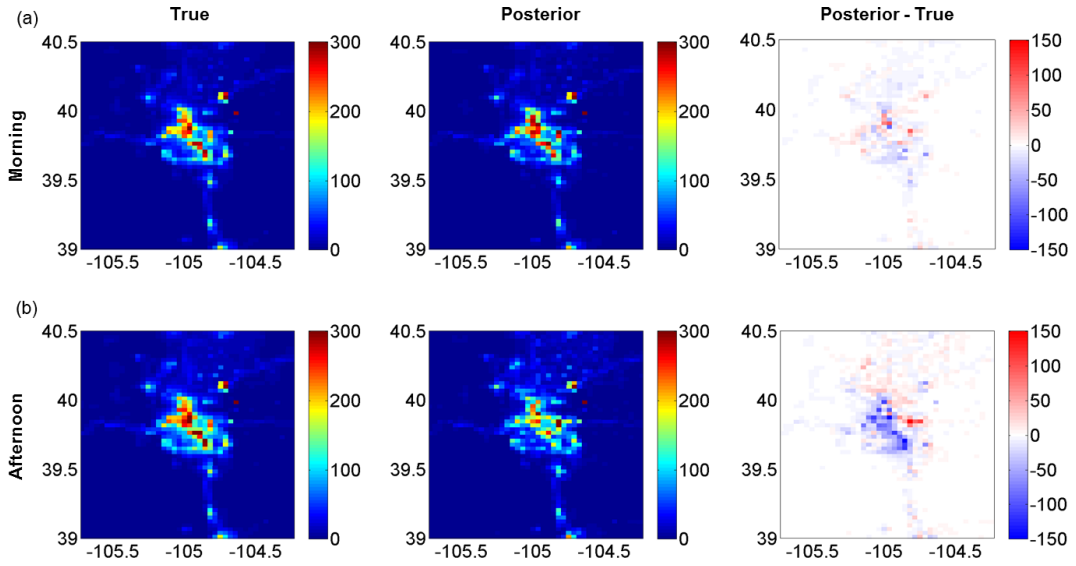

Figure 8. The emission estimation results in ENS.1 at 09:00 MST **(a)** and 16:00 MST **(b)** on 3 July of true and posterior emissions and the difference between true and posterior emissions (from left to right). The unit is mol km^{-2} h^{-1}.

poral resolution to make use of them in the assimilation. In the coupled chemical and meteorological data assimilation system, we apply an OSSE framework to estimate NO_x emissions in Denver by jointly assimilating MADIS observation of meteorological variables as well as future TEMPO NO_2 columns. In the meteorological assimilation we successfully reduced the posterior wind RMSE below 0.5 m s^{-1} in Denver to better represent the NO_2 transport. The prior wind RMSE and spread show peaks in the afternoon, thus increasing the errors in NO_2 transport. We find that the meteorological uncertainties contribute 35 % to the total NO_2 forecast uncertainties, considering the emission uncertainties of 60 %. Assimilation of TEMPO NO_2 columns reduces errors in the predicted NO_2 concentration by more than 50 %, which demonstrates the potential of future geostationary observations to constrain the NO_2 chemical weather.

One of the goals of this work is to investigate the optimal strategy to estimate NO_x emissions. We test the upper limit of emission constraints from TEMPO NO_2 observations in an ideal case assuming no errors associated with the modeled meteorology. In the experiment of joint assimilation of meteorology and chemical NO_2, we find that the estimate of emissions is most successful in the morning but degrades in the afternoon when the prior wind RMSE grows above 1 m s^{-1}. Considering the dependence of errors in estimated emissions on the wind forecast errors, we recommend guaranteeing the accuracy in modeled wind and achieving a wind RMSE below 1 m s^{-1} for the success of chemical assimilation in inferring emissions at the 3 km scale of our model grid. We show that the simultaneous update of NO_x emissions and concentrations outperforms the approach of updating emissions only. We recommend carrying out meteorology assimilations to stabilize from the initial transport errors before starting the emission inversion.

We would like to point out that the covariance of error statistics between wind and NO_2 are not utilized in the OSSE assimilation in this paper. Results on carbon and weather assimilation show that the variable localization scheme zeroes out the background error covariance among prognostic variables that are not physically related, thus reducing sampling errors (Kang et al., 2011). Specifically, they find that covariance between carbon fluxes and meteorological variables should be neglected. However, the same result might not be obtained for short-lived chemicals. The extent to which chemical observations can be used to improve the assimilation of meteorological variables and vice-versa in a situation where we do not zero the covariance in the errors should be pursued in future research.

Data availability. No data sets were used in this article.

Competing interests. The authors declare that they have no conflict of interest.

Acknowledgements. The authors gratefully acknowledge support from the NASA grants NNX14AH046, NNX15AE376, and NSF1352972. We thank N. Collins (NCAR/IMAGe) and T. Hoar (NCAR/IMAGe) for the assistance with DART. We would like to acknowledge high-performance computing support from Yellowstone (ark:/85065/d7wd3xhc) provided by NCAR's Computational and Information Systems Laboratory, sponsored by the National Science Foundation. We also thank the reviewers of this paper for their constructive suggestions.

Edited by: Q. Zhang
Reviewed by: two anonymous referees

References

Aksoy, A., Zhang, F. and Nielsen-Gammon, J. W.: Ensemble-Based Simultaneous State and Parameter Estimation in a Two-Dimensional Sea-Breeze Model, Mon. Weather Rev., 134, 2951–2970, https://doi.org/10.1175/MWR3224.1, 2006.

Anderson, J., Hoar, T., Raeder, K., Liu, H., Collins, N., Torn, R., and Avellano, A.: The Data Assimilation Research Testbed: A Community Facility, Bull. Am. Meteorol. Soc., 90, 1283–1296, https://doi.org/10.1175/2009BAMS2618.1, 2009.

Anderson, J. L.: An Ensemble Adjustment Kalman Filter for Data Assimilation, Mon. Weather Rev., 129, 2884–2902, 2001.

Anderson, J. L. and Collins, N.: Scalable Implementations of Ensemble Filter Algorithms for Data Assimilation, J. Atmos. Ocean. Tech., 24, 1452–1463, https://doi.org/10.1175/JTECH2049.1, 2007.

Arellano Jr., A. F., Raeder, K., Anderson, J. L., Hess, P. G., Emmons, L. K., Edwards, D. P., Pfister, G. G., Campos, T. L., and Sachse, G. W.: Evaluating model performance of an ensemble-based chemical data assimilation system during INTEX-B field mission, Atmos. Chem. Phys., 7, 5695–5710, https://doi.org/10.5194/acp-7-5695-2007, 2007.

Barbu, A. L., Segers, A. J., Schaap, M., Heemink, A. W., and Builtjes, P. J. H.: A multi-component data assimilation experiment directed to sulphur dioxide and sulphate over Europe, Atmos. Environ., 43, 1622–1631, https://doi.org/10.1016/j.atmosenv.2008.12.005, 2009.

Barker, D., Huang, X.-Y., Liu, Z., Auligné, T., Zhang, X., Rugg, S., Ajjaji, R., Bourgeois, A., Bray, J., Chen, Y., Demirtas, M., Guo, Y.-R., Henderson, T., Huang, W., Lin, H.-C., Michalakes, J., Rizvi, S., and Zhang, X.: The Weather Research and Forecasting Model's Community Variational/Ensemble Data Assimilation System: WRFDA, Bull. Am. Meteorol. Soc., 93, 831–843, https://doi.org/10.1175/BAMS-D-11-00167.1, 2012.

Barré, J., Gaubert, B., Arellano, A. F. J., Worden, H. M., Edwards, D. P., Deeter, M. N., Anderson, J. L., Raeder, K., Collins, N., Tilmes, S., Francis, G., Clerbaux, C., Emmons, L. K., Pfister, G. G., Coheur, P.-F., and Hurtmans, D.: Assessing the impacts of assimilating IASI and MOPITT CO retrievals using CESM-CAM-chem and DART, J. Geophys. Res.-Atmos., 120, 10501–10529, https://doi.org/10.1002/2015JD023467, 2015.

Beirle, S., Boersma, K. F., Platt, U., Lawrence, M. G., and Wagner, T.: Megacity emissions and lifetimes of nitrogen oxides probed from space, Science, 333, 1737–9, https://doi.org/10.1126/science.1207824, 2011.

Boersma, K. F., Eskes, H. J., and Brinksma, E. J.: Error analysis for tropospheric NO_2 retrieval from space, J. Geophys. Res., 109, D04311, https://doi.org/10.1029/2003JD003962, 2004.

Bousserez, N., Henze, D. K., Rooney, B., Perkins, A., Wecht, K. J., Turner, A. J., Natraj, V., and Worden, J. R.: Constraints on methane emissions in North America from future geostationary remote sensing measurements, Atmos. Chem. Phys., 16, 6175–6190, https://doi.org/10.5194/acp-16-6175-2016, 2016.

Bowman, K. W.: Toward the next generation of air quality monitoring: Ozone, Atmos. Environ., 80, 571–583, https://doi.org/10.1016/j.atmosenv.2013.07.007, 2013.

Bucsela, E. J., Krotkov, N. A., Celarier, E. A., Lamsal, L. N., Swartz, W. H., Bhartia, P. K., Boersma, K. F., Veefkind, J. P., Gleason, J. F., and Pickering, K. E.: A new stratospheric and tropospheric NO_2 retrieval algorithm for nadir-viewing satellite instruments: applications to OMI, Atmos. Meas. Tech., 6, 2607–2626, https://doi.org/10.5194/amt-6-2607-2013, 2013.

Chatterjee, A., Michalak, A. M., Anderson, J. L., Mueller, K. L., and Yadav, V.: Toward reliable ensemble Kalman filter estimates of CO_2 fluxes, J. Geophys. Res.-Atmos., 117, 1–17, https://doi.org/10.1029/2012JD018176, 2012.

Claeyman, M., Attié, J.-L., Peuch, V.-H., El Amraoui, L., Lahoz, W. A., Josse, B., Ricaud, P., von Clarmann, T., Höpfner, M., Orphal, J., Flaud, J.-M., Edwards, D. P., Chance, K., Liu, X., Pasternak, F., and Cantié, R.: A geostationary thermal infrared sensor to monitor the lowermost troposphere: O_3 and CO retrieval studies, Atmos. Meas. Tech., 4, 297–317, https://doi.org/10.5194/amt-4-297-2011, 2011.

Cui, Y. Y., Brioude, J., McKeen, S. A., Angevine, W. M., Kim, S.-W., Frost, G. J., Ahmadov, R., Peischl, J., Bousserez, N., Liu, Z., and Ryerson, T. B.: Top-down estimate of methane emissions in California using a mesoscale inverse modeling technique: The South Coast Air Basin, J. Geophys. Res. Atmos., 120, 6698–6711, https://doi.org/10.1002/2014JD023002, 2015.

Edwards, D. P., Arellano, A. F., and Deeter, M. N.: A satellite observation system simulation experiment for carbon monoxide in the lowermost troposphere, J. Geophys. Res., 114, D14304, https://doi.org/10.1029/2008JD011375, 2009.

Elbern, H., Strunk, A., Schmidt, H., and Talagrand, O.: Emission rate and chemical state estimation by 4-dimensional variational inversion, Atmos. Chem. Phys., 7, 3749–3769, https://doi.org/10.5194/acp-7-3749-2007, 2007.

Evensen, G.: The ensemble Kalman Filter: theoretical formulation and practical implementation, Ocean Dynam., 53, 343–367, 2003.

Fishman, J., Iraci, L. T., Al-Saadi, J., Chance, K., Chavez, F., Chin, M., Coble, P., Davis, C., DiGiacomo, P. M., Edwards, D., Eldering, A., Goes, J., Herman, J., Hu, C., Jacob, D. J., Jordan, C., Kawa, S. R., Key, R., Liu, X., Lohrenz, S., Mannino, A., Natraj, V., Neil, D., Neu, J., Newchurch, M., Pickering, K., Salisbury, J., Sosik, H., Subramaniam, A., Tzortziou, M., Wang, J., and Wang, M.: The United States' Next Generation of Atmospheric Composition and Coastal Ecosystem Measurements: NASA's Geostationary Coastal and Air Pollution Events (GEO-CAPE) Mission, Bull. Am. Meteorol. Soc., 93, 1547–1566, https://doi.org/10.1175/BAMS-D-11-00201.1, 2012.

Gaspari, G., Gaspari, G., Cohn, S. E., and Cohn, S. E.: Construction of correlation functions in two and three dimensions, Q. J. R. Meteorol. Soc., 125, 723–757, https://doi.org/10.1002/qj.49712555417, 1999.

Gaubert, B., Coman, A., Foret, G., Meleux, F., Ung, A., Rouil, L., Ionescu, A., Candau, Y., and Beekmann, M.: Regional scale ozone data assimilation using an ensemble Kalman filter and the CHIMERE chemical transport model, Geosci. Model Dev., 7, 283–302, https://doi.org/10.5194/gmd-7-283-2014, 2014.

Guerrette, J. J. and Henze, D. K.: Development and application of the WRFPLUS-Chem online chemistry adjoint and WRFDA-

Chem assimilation system, Geosci. Model Dev., 8, 1857–1876, https://doi.org/10.5194/gmd-8-1857-2015, 2015.

Hache, E., Attié, J.-L., Tourneur, C., Ricaud, P., Coret, L., Lahoz, W. A., El Amraoui, L., Josse, B., Hamer, P., Warner, J., Liu, X., Chance, K., Höpfner, M., Spurr, R., Natraj, V., Kulawik, S., Eldering, A., and Orphal, J.: The added value of a visible channel to a geostationary thermal infrared instrument to monitor ozone for air quality, Atmos. Meas. Tech., 7, 2185–2201, https://doi.org/10.5194/amt-7-2185-2014, 2014.

Houtekamer, P. L. and Mitchell, H. L.: A sequential ensemble Kalman filter for atmospheric data assimilation, Mon. Weather Rev., 129, 123–137, 2001.

Hu, X.-M., Nielsen-Gammon, J. W., and Zhang, F.: Evaluation of Three Planetary Boundary Layer Schemes in the WRF Model, J. Appl. Meteorol. Climatol., 49, 1831–1844, https://doi.org/10.1175/2010JAMC2432.1, 2010.

Kang, J.-S., Kalnay, E., Liu, J., Fung, I., Miyoshi, T., and Ide, K.: "Variable localization" in an ensemble Kalman filter: Application to the carbon cycle data assimilation, J. Geophys. Res., 116, D09110, https://doi.org/10.1029/2010JD014673, 2011.

Kang, J.-S., Kalnay, E., Miyoshi, T., Liu, J., and Fung, I.: Estimation of surface carbon fluxes with an advanced data assimilation methodology, J. Geophys. Res.-Atmos., 117, D24101, https://doi.org/10.1029/2012JD018259, 2012.

Koohkan, M. R., Bocquet, M., Roustan, Y., Kim, Y., and Seigneur, C.: Estimation of volatile organic compound emissions for Europe using data assimilation, Atmos. Chem. Phys., 13, 5887–5905, https://doi.org/10.5194/acp-13-5887-2013, 2013.

Kretschmer, R., Gerbig, C., Karstens, U., and Koch, F.-T.: Error characterization of CO_2 vertical mixing in the atmospheric transport model WRF-VPRM, Atmos. Chem. Phys., 12, 2441–2458, https://doi.org/10.5194/acp-12-2441-2012, 2012.

Kretschmer, R., Gerbig, C., Karstens, U., Biavati, G., Vermeulen, A., Vogel, F., Hammer, S., and Totsche, K. U.: Impact of optimized mixing heights on simulated regional atmospheric transport of CO_2, Atmos. Chem. Phys., 14, 7149–7172, https://doi.org/10.5194/acp-14-7149-2014, 2014.

Krotkov, N. A., McLinden, C. A., Li, C., Lamsal, L. N., Celarier, E. A., Marchenko, S. V., Swartz, W. H., Bucsela, E. J., Joiner, J., Duncan, B. N., Boersma, K. F., Veefkind, J. P., Levelt, P. F., Fioletov, V. E., Dickerson, R. R., He, H., Lu, Z., and Streets, D. G.: Aura OMI observations of regional SO_2 and NO_2 pollution changes from 2005 to 2014, Atmos. Chem. Phys., 16, 4605–4629, https://doi.org/10.5194/acp-16-4605-2016, 2016.

Lahoz, W. A., Peuch, V.-H., Orphal, J., Attié, J.-L., Chance, K., Liu, X., Edwards, D., Elbern, H., Flaud, J.-M., Claeyman, M., and Amraoui, L. El: Monitoring Air Quality from Space: The Case for the Geostationary Platform, Bull. Am. Meteorol. Soc., 93, 221–233, https://doi.org/10.1175/BAMS-D-11-00045.1, 2012.

Laughner, J. L., Zare, A., and Cohen, R. C.: Effects of daily meteorology on the interpretation of space-based remote sensing of NO_2, Atmos. Chem. Phys., 16, 15247–15264, https://doi.org/10.5194/acp-16-15247-2016, 2016.

Lauvaux, T. and Davis, K. J.: Planetary boundary layer errors in mesoscale inversions of column-integrated CO_2 measurements, J. Geophys. Res.-Atmos., 119, 490–508, https://doi.org/10.1002/2013JD020175, 2014.

Liu, J., Fung, I., Kalnay, E., and Kang, J.-S.: CO_2 transport uncertainties from the uncertainties in meteorological fields, Geophys. Res. Lett., 38, L12808, https://doi.org/10.1029/2011GL047213, 2011.

Miyazaki, K., Eskes, H. J., Sudo, K., Takigawa, M., van Weele, M., and Boersma, K. F.: Simultaneous assimilation of satellite NO_2, O_3, CO, and HNO_3 data for the analysis of tropospheric chemical composition and emissions, Atmos. Chem. Phys., 12, 9545–9579, https://doi.org/10.5194/acp-12-9545-2012, 2012.

Miyazaki, K., Eskes, H., Sudo, K., Boersma, K. F., Bowman, K., and Kanaya, Y.: Decadal changes in global surface NO_x emissions from multi-constituent satellite data assimilation, Atmos. Chem. Phys., 17, 807–837, https://doi.org/10.5194/acp-17-807-2017, 2017.

Mizzi, A. P., Arellano Jr., A. F., Edwards, D. P., Anderson, J. L., and Pfister, G. G.: Assimilating compact phase space retrievals of atmospheric composition with WRF-Chem/DART: a regional chemical transport/ensemble Kalman filter data assimilation system, Geosci. Model Dev., 9, 965–978, https://doi.org/10.5194/gmd-9-965-2016, 2016.

Pagowski, M. and Grell, G. A.: Experiments with the assimilation of fine aerosols using an ensemble Kalman filter, J. Geophys. Res.-Atmos., 117, D21302, https://doi.org/10.1029/2012JD018333, 2012.

Romine, G. S., Schwartz, C. S., Snyder, C., Anderson, J. L., and Weisman, M. L.: Model Bias in a Continuously Cycled Assimilation System and Its Influence on Convection-Permitting Forecasts, Mon. Weather Rev., 141, 1263–1284, https://doi.org/10.1175/MWR-D-12-00112.1, 2013.

Russell, A. R., Perring, A. E., Valin, L. C., Bucsela, E. J., Browne, E. C., Wooldridge, P. J., and Cohen, R. C.: A high spatial resolution retrieval of NO_2 column densities from OMI: method and evaluation, Atmos. Chem. Phys., 11, 8543–8554, https://doi.org/10.5194/acp-11-8543-2011, 2011.

Russell, A. R., Valin, L. C., and Cohen, R. C.: Trends in OMI NO_2 observations over the United States: effects of emission control technology and the economic recession, Atmos. Chem. Phys., 12, 12197–12209, https://doi.org/10.5194/acp-12-12197-2012, 2012.

Saide, P. E., Kim, J., Song, C. H., Choi, M., Cheng, Y., and Carmichael, G. R.: Assimilation of next generation geostationary aerosol optical depth retrievals to improve air quality simulations, Geophys. Res. Lett., 41, 9188–9196, https://doi.org/10.1002/2014GL062089.Received, 2014.

Stockwell, W. R., Middleton, P., Chang, J. S., and Tang, X.: The second generation regional acid deposition model chemical mechanism for regional air quality modeling, J. Geophys. Res., 95, 16343, https://doi.org/10.1029/JD095iD10p16343, 1990.

Travis, K. R., Jacob, D. J., Fisher, J. A., Kim, P. S., Marais, E. A., Zhu, L., Yu, K., Miller, C. C., Yantosca, R. M., Sulprizio, M. P., Thompson, A. M., Wennberg, P. O., Crounse, J. D., St. Clair, J. M., Cohen, R. C., Laugher, J. L., Dibb, J. E., Hall, S. R., Ullmann, K., Wolfe, G. M., Pollack, I. B., Peischl, J., Neuman, J. A., and Zhou, X.: NO_x emissions, isoprene oxidation pathways, vertical mixing, and implications for surface ozone in the Southeast United States, Atmos. Chem. Phys., 16, 13561–13577, https://doi.org/10.5194/acp-16-13561-2016, 2016.

Turner, A. J., Jacob, D. J., Wecht, K. J., Maasakkers, J. D., Lundgren, E., Andrews, A. E., Biraud, S. C., Boesch, H., Bowman, K. W., Deutscher, N. M., Dubey, M. K., Griffith, D. W. T., Hase, F., Kuze, A., Notholt, J., Ohyama, H., Parker, R., Payne, V.

H., Sussmann, R., Sweeney, C., Velazco, V. A., Warneke, T., Wennberg, P. O., and Wunch, D.: Estimating global and North American methane emissions with high spatial resolution using GOSAT satellite data, Atmos. Chem. Phys., 15, 7049–7069, https://doi.org/10.5194/acp-15-7049-2015, 2015.

Valin, L. C., Russell, A. R., Hudman, R. C., and Cohen, R. C.: Effects of model resolution on the interpretation of satellite NO_2 observations, Atmos. Chem. Phys., 11, 11647–11655, https://doi.org/10.5194/acp-11-11647-2011, 2011.

Valin, L. C., Russell, A. R., and Cohen, R. C.: Variations of OH radical in an urban plume inferred from NO_2 column measurements, Geophys. Res. Lett., 40, 1856–1860, https://doi.org/10.1002/grl.50267, 2013.

Yumimoto, K.: Impacts of geostationary satellite measurements on CO forecasting: An observing system simulation experiment with GEOS-Chem/LETKF data assimilation system, Atmos. Environ., 74, 123–133, https://doi.org/10.1016/j.atmosenv.2013.03.032, 2013.

Zoogman, P., Jacob, D. J., Chance, K., Worden, H. M., Edwards, D. P., and Zhang, L.: Improved monitoring of surface ozone by joint assimilation of geostationary satellite observations of ozone and CO, Atmos. Environ., 84, 254–261, https://doi.org/10.1016/j.atmosenv.2013.11.048, 2014.

Zoogman, P., Liu, X., Suleiman, R. M., Pennington, W. F., Flittner, D. E., Al-Saadi, J. A., Hilton, B. B., Nicks, D. K., Newchurch, M. J., Carr, J. L., Janz, S. J., Andraschko, M. R., Arola, A., Baker, B. D., Canova, B. P., Chan Miller, C., Cohen, R. C., Davis, J. E., Dussault, M. E., Edwards, D. P., Fishman, J., Ghulam, A., González Abad, G., Grutter, M., Herman, J. R., Houck, J., Jacob, D. J., Joiner, J., Kerridge, B. J., Kim, J., Krotkov, N. A., Lamsal, L., Li, C., Lindfors, A., Martin, R. V., McElroy, C. T., McLinden, C., Natraj, V., Neil, D. O., Nowlan, C. R., O'Sullivan, E. J., Palmer, P. I., Pierce, R. B., Pippin, M. R., Saiz-Lopez, A., Spurr, R. J. D., Szykman, J. J., Torres, O., Veefkind, J. P., Veihelmann, B., Wang, H., Wang, J., and Chance, K.: Tropospheric emissions: Monitoring of pollution (TEMPO), J. Quant. Spectrosc. Radiat. Transf., 186, 17–39, https://doi.org/10.1016/j.jqsrt.2016.05.008, 2017.